ORIGINAL PAPER

Theoretical studies on the tautomerism and intramolecular hydrogen shifts of 5-Amino-tetrazole in the gas phase

Jian-Guo Zhang · Li-Na Feng · Yuan-Jie Shu · Shao-Wen Zhang · Tong-Lai Zhang · Li Yang · Man Wu

Abstract The tautomerism and intramolecular hydrogen shifts of 5-amino-tetrazole in the gas phase were studied in the present work. The minimum energy path (MEP) information of 5-amino-tetrazole was obtained at the CCSD(T)/6–311G**//MP2/6–311G** level of theory. The six possible tautomers of 1H, 4H-5-imino-tetrazole (**a**), 1H-5-amino-tetrazole (**b**), 2H-5-amino-tetrazole (**c**), 1H, 2H-5-imino-tetrazole (**d**), the mesoionic form (**e**) and 2H, 4H-5-imino-tetrazole (**f**) were investigated. Among these tautomers, there are 2 amino- forms, 3 imino- forms, and 1 mesoionic structure form. In all the tautomers, 2-H form (**c**) is the energetically preferred one in the gas phase. In the imino- tautomers, the energy value of the compound **d** is similar as that of the compound **f** but it is higher than the energy value of the compound **a**. The potential energetic surface (PES) and kinetics for five reactions have been investigated. Reaction 2 (**b→c**) was hydrogen shifts only in which the 1-H and 2-H rearrangement. This means that the reaction 2 (**b→c**) is energetically favorable having an activation barrier of 45.66 kcal·mol^{-1} and the reaction energies (ΔE) is only 2.67 kcal·mol^{-1}. However, the reaction energy barrier for tautomerism of reaction 1 (**b→e**) is 54.90 kcal·mol^{-1}. Reaction 1 (**b→a**), reaction 3 (**c→d**), and reaction 5 (**c→f**) were amino- →imino- tautomerism reactions. The energy barriers of amino- →imino- tautomerism reactions required are 59.39, 65.57, 73.61 kcal·mol^{-1} respectively in the gas phase. The calculated values of rate constants using TST, TST/Eckart, CVT, CVT/SCT and CVT/ZCT methods using the optimized geometries obtained at the MP2/6–311G** level of theory show the variational effects are small over the whole temperature range, while tunneling effects are big in the lower temperature range for all tautomerism reactions.

Keywords 5-amino-tetrazole · Intramolecular hydrogen shifts · Kinetics · Tautomerism · Tunneling effect

J.-G. Zhang (✉) · L.-N. Feng · T.-L. Zhang · L. Yang · M. Wu
State Key Laboratory of Explosion Science and Technology,
Beijing Institute of Technology,
Beijing 100081, People's Republic of China
e-mail: zhangjianguobit@yahoo.com.cn

L.-N. Feng
Shanxi Fenxi Heavy Industry Co., Ltd.,
Taiyuan 030027, People's Republic of China

Y.-J. Shu
Institute of Chemical Materials,
Chinese Academy of Engineering Physics (CAEP),
Mianyang 621900, People's Republic of China

S.-W. Zhang
School of Science, Beijing Institute of Technology,
Beijing 100081, People's Republic of China

Introduction

As high nitrogen content-high energy materials (HNC-HEM), tetrazoles are widely used in many areas. They have a high content of nitrogen so that they are used in energetic materials [1]. They can also be used as a gas generator and key intermediate in many organic synthesis [2]. There is considerable interest in the medicinal and biological applications of tetrazoles, too.

The theoretical prediction of the tautomerization energy of tetrazoles in gas phase has attracted intense interest of energetic material workers in the past years. In particular, a series of experimental and theoretical attempts have been devoted to the intriguing phenomenon of tetrazoles' tautomerism using highly accurate methods [3, 4]. Levchik found that 5-amino-tetrazole (ATZ) existed mainly in the imino- form in the solid state[5]. 1H, 4H-5-imino-tetrazole (**a**) was identified with IR spectroscopy technology[6, 7].

However, Murphy et al. had demonstrated that the tautomeric equilibrium from amino- (**b**) to imino- (**a**) would not be expected to exist under the experimental conditions in the solid[8], and other people thought that solid monohydrate of ATZ exists in the amino-form (**b**) with a strong hydrogen bonding between the nitrogen atoms of the cycle and water molecules[9]. In the DMF solution, ATZ predominately existed in the imino- form (**a**) according to the NMR data, while in the solution of dimethyl sulfoxide it was mainly in the form **b** [10]. Whereas, in the toluene or CCl₄ solution, there were resonance peaks attributed to both amino- (**b**) and imino- (**a**) forms [11]. In the solid state, amino- tautomer (**b**) was detected clearly from X-ray crystallography [12]. The MRCI study showed the 2H- (**c**) tautomer was more stable than the 1H- (**b**) form by 99 kJ/mol [13] in the gas phase, while Ming showed the MRCI value overestimated the relative energy [14]. Xiao and his co-workers [4, 15–18] studied tetrazoles largely, however they did not give the detailed investigation results of the kinetics for ATZ. There are no further experiments and calculations have been performed according to our knowledge. Which form does ATZ exit on earth usually? It is therefore necessary to quantify the competition among all the possible hydrogen shift reactions. The tautomers and reactions of the tautomerism of 5-amino-tetrazole (ATZ) in the gas phase are shown in Fig. 1.

This paper focuses on the tautomers and intramolecular hydrogen shifts of ATZ and their kinetics in the gas phase. Our study aims to determine the stability of the tautomers and the mechanism of these tautomerism reactions, obtain more kinetic information and evaluate the rate constants over a wide temperature range.

Computational methods

All the calculations were carried out with the Gaussian 03 program [19]. The geometries and frequencies of reactants, products, and transition states were optimized using MP2 method[20, 21] with 6–311G** basis set[22, 23]. To yield a more reliable enthalpy and barrier height, we made single-point energy calculations for the stationary points through CCSD(T) calculations [24, 25] with 6–311G** basis set. The minimum energy path (MEP) was obtained using the intrinsic reaction coordinate (IRC) method[26] at the MP2/6–311G** level of theory. The IRC calculations proved the reaction paths leading down from a transition structure on a potential energy surface. 150 points for both side were calculated from the transition states folling the MEP with a gradient step size of 0.02(amu)$^{1/2}$ bohr. In addition, the energy derivatives, including gradients and Hessians matrix at geometries of some selected points along the minimum energy path (MEP) were calculated at the same level.
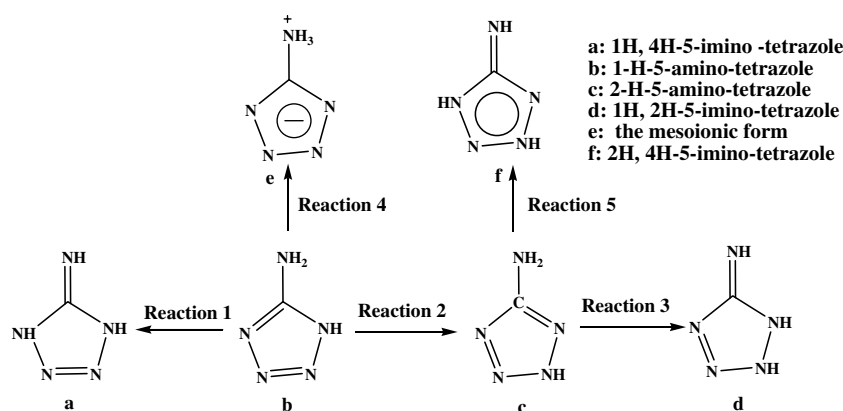
In the calculation of rate constants, the single-point energy calculations for the stationary points along the MEP were refined to establish the electronic potential curve with the CCSD(T)/6–311G** level of theory too. Kinetics calculations of these reactions were carried on the basis of this initial information (optimized geometries, energies, gradients, and frequencies analysis along the MEP) by means of Vklab program package [27] and POLYRATE 8.2 program [28]. All of the rate constants reported here were evaluated over a wide temperature region from 200 to 2500 K using the conventional, non-variational transition-state theory (TST)[29], the TST rate constant calculations with the Eckart tunneling correction (TST/Eckart)[30], the canonical variational transition-state theory (CVT)[31–33], canonical variational transition-state theory with small curvature tunneling correction (CVT/SCT) [34, 35], and canonical variational transition-state theory with zero- curvature tunneling correction (CVT/ZCT) [36].

Results and discussion

The comparison of geometries and energies

The mechanisms of tautomerism reactions for ATZ are shown in Fig. 2. The optimized structures containing the

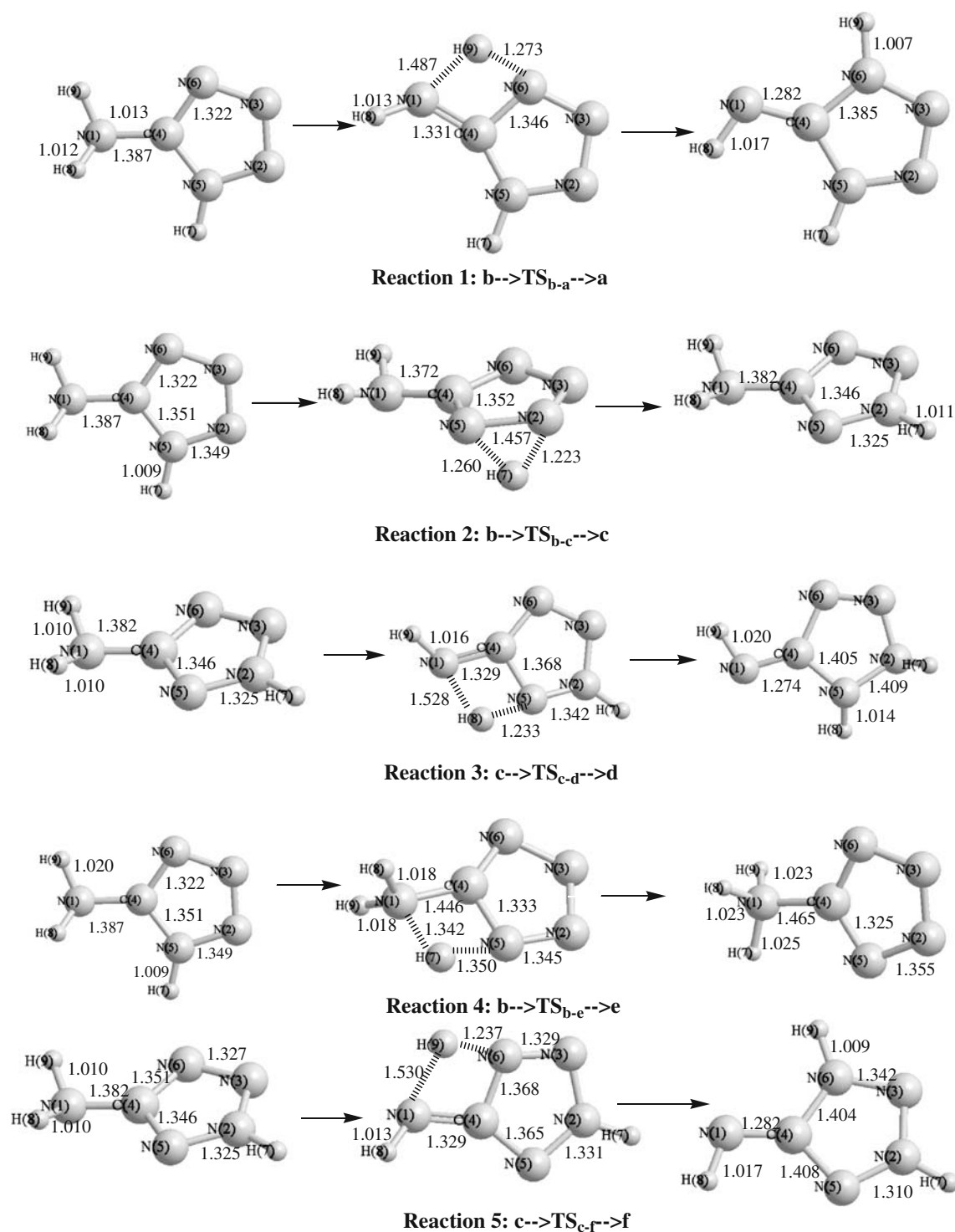Fig. 1 The tautomers and reactions of the tautomerism of 5-amino-tetrazole (ATZ) in the gas phase

a: 1H, 4H-5-imino -tetrazole
b: 1-H-5-amino-tetrazole
c: 2-H-5-amino-tetrazole
d: 1H, 2H-5-imino-tetrazole
e: the mesoionic form
f: 2H, 4H-5-imino-tetrazole

Reaction 1: b-->TS$_{b-a}$-->a

Reaction 2: b-->TS$_{b-c}$-->c

Reaction 3: c-->TS$_{c-d}$-->d

Reaction 4: b-->TS$_{b-e}$-->e

Reaction 5: c-->TS$_{c-f}$-->f

Fig. 2 The mechanism of the tautomeric equilibrium and hydrogen shifts for ATZ

main bond parameters at the MP2/6–311G** level of theory for the reactants, products and transition states are given in Table 1.

The experimental C = N bond length is 1.273 Å in $H_2C = NH$ and the C-N bond length is 1.474 Å in CH_3NH_2[37]. For comparison, in the imino-forms (**a**, **d**, and **f**), the C_4-N_1

bonds length calculated of **a** and **f** are 1.282 Å and the one of **d** is 1.274 Å, which are close to a double bond character. For **a**, the C_4-N_5 and C_4-N_6 bond length calculated are 1.391 Å and 1.385 Å, it can be inferred that these two bonds are between single bonds and double bonds. The N-N distances in the H-N = N-H and H_2N-NH_2 are 1.252 and

Table 1 Some optimized geometries of tautomers of ATZ and the transition states at MP2/6–311G** (bond lengths are given in angstroms and bond angles in degrees)

Species Para.	b	TS$_{b-a}$	a	TS$_{b-c}$	c	TS$_{c-d}$	d	TS$_{b-e}$	e	TS$_{c-f}$	f
R(1,4)	1.387	1.331	1.282	1.372	1.382	1.329	1.274	1.446	1.465	1.329	1.282
R(2,3)	1.311	1.306	1.288	1.329	1.333	1.346	1.366	1.341	1.339	1.341	1.326
R(2,5)	1.349	1.378	1.361	1.457	1.325	1.342	1.409	1.345	1.355	1.331	1.310
R(3,6)	1.360	1.347	1.352	1.330	1.327	1.316	1.272	1.368	1.359	1.329	1.342
R(4,5)	1.351	1.350	1.391	1.352	1.346	1.368	1.405	1.333	1.325	1.365	1.408
R(4,6)	1.322	1.346	1.385	1.344	1.351	1.376	1.435	1.317	1.321	1.368	1.404
A(3,2,5)	105.50	107.22	107.26	108.15	115.96	110.52	107.48	106.09	109.93	118.94	119.65
A(2,3,6)	111.18	107.74	107.65	109.98	104.70	108.32	110.79	112.12	110.05	100.03	99.59
A(1,4,5)	124.39	147.89	135.80	123.52	123.34	106.90	125.04	102.49	119.68	144.69	133.02
A(5,4,6)	108.08	104.10	98.44	112.73	113.22	109.54	105.79	114.51	117.89	108.80	103.31
A(2,5,4)	109.16	109.62	113.09	101.80	99.86	102.86	104.31	105.81	101.16	100.22	103.43
A(3,6,4)	106.07	110.95	113.55	106.89	106.27	106.04	108.82	101.46	100.98	111.48	114.01

1.449 Å[36], respectively. The N_2-N_3 bond length calculated of **a** is 1.288 Å, the N_2-N_5 and N_3-N_6 bond length are 1.361 Å and 1.352 Å, so the length of N-N bonds of **a** are between single bonds and double bonds obviously, while the N_2-N_3 bond is near to a double bond, the other N-N bonds are inclined to single bonds. For **d**, it is very similar but the C_4-N_5 and C_4–N_6 display the single bond. The N_2–N_3 bond length calculated for **d** is 1.366 Å, the N_2–N_5 bond length is 1.409 Å, the N_3–N_6 bond length is 1.272 Å, so the lengths of C-N bonds and N-N bonds of **d** are between single bonds and double bonds except N_3–N_6 and C_4–N_1 are closer to a double bond, N_2–N_5 is closer to a single bond. As for **f**, the C_4–N_5 and C_4–N_6 bond length calculated are 1.408 Å and 1.404 Å, they are closer to single bonds. The N_2–N_3, N_2–N_5, and N_3–N_6 bond length calculated for **f** are 1.326 Å, 1.310 Å, and 1.342 Å, respectively, which suggest that these three bonds of the ring are between single bonds and double bonds while inclined to double bonds.

For six tautomers, all the non-hydrogen atoms are in a plane excellently except **d**. For the amino-forms, the C_4-N_1 bond length calculated for **b** and **c** are 1.387 Å and 1.382 Å, other C-N and N-N bond length in the framework for **b** and **c** are in the range of 1.311 Å ~ 1.360 Å in the MP2/6-311G** level of theory, which lie between those of isolated single and double bonds. The results clearly indicated that the lone pair electrons at N_5 in the **b** and N_2 in the **c** are delocalized in planer five-center 6π electron aromatic systems, indicating that the molecules are aromatic. This may be the reason for which **b** and **c** are more stable.

For the mesoionic form (**e**), the C_4-N_1 bond length calculated is 1.465 Å. This displays a typical single bond character. The C_4–N_5 and C_4–N_6 bond length calculated are 1.325 Å and 1.321Å, which are closer to double bonds. However, the N_2–N_3, N_2–N_5, and N_3–N_6 bond length for the compound **e** are 1.339 Å, 1.355 Å, and 1.359Å. These

three bonds of the ring have between single and double bond character, which follows the average.

The calculated enthalpies, and zero-point vibrational energies with MP2/6–311G** method and relative energy with CCSD(T) /6–311G**//MP2/6–311G** method are presented in Table 2. From the relative energy data, we can find the 2-H form (**c**) is the energetically preferred one in the gas phase among all the tautomers. Since the amino-tautomers (compound **b** and **c**) have relatively much lower energy than the imino- tautomers, we think of the existence of aromatic systems forming the conjugation effect in the compounds of **b** and **c**. In addition, the calculations in this paper also show **c** is more stable than **b** by 2.67 kcal/mol, which is in accordance with reference [38] results. In the imino- tautomers, the energy value of compound **d** is similar to that of the compound **f** but it is higher than the energy value of compound **a**. The energy value of the mesoionic form (**e**) is remarkably higher than other tautomers.

Vibrational frequencies and infrared spectra

The harmonic vibrational frequencies were calculated to confirm the stationary nature and make zero-point energy

Table 2 Enthalpies [a], zero-point vibrational energies [a] (ZPE), and relative energies [b] (take b as standard) of the tautomers of ATZ (in kcal/mol)

Species Para.	a	b	c	d	e	f
Enthalpies	13.16	0.00	−4.74	32.15	31.06	23.89
ZPE	39.86	40.44	40.80	40.08	40.80	40.48
Relative energies	11.16	0.00	−2.67	26.71	33.42	26.72

[a] based on MP2/6–311G**, [b] based on refined energies(CCSD(T)/6–311G**) and ZPE(MP2/6–311G**)

(ZPE) corrections at the MP2/6–311G** level. All of the minima including six tautomers possess only real frequencies, and all the force constant eigenvalues are positive. We have reported the infrared spectra of all six tautomers and the transition states of the tautomeric equilibrium of hydrogen shifts in Table 3. The most often observed molecular geometry of ATZ is **b**, the most stable is **c,** so in this paper we take **b** and **c** as standards for the farther depiction. **Reaction 1** is hydrogen on N_1 shifts to N_6, namely tautomerism of **b** to **a**. **Reaction 2** is hydrogen on N_5 shifts to N_2, namely tautomerism of **b** to **c**. **Reaction 3** is hydrogen on N_1 shifts to N_5, namely tautomerism of **c** to **d**. **Reaction 4** is hydrogen on N_5 shifts to N_1, namely tautomerism of **b** to **e**. **Reaction 5** is hydrogen on N_1 shifts to N_6, namely tautomerism of **c** to **f**. The detailed mechanism for **Reactions 1-5** can be found in Fig. 2. TS_{b-a}, TS_{b-c}, TS_{c-d}, TS_{b-e}, TS_{c-f} are the transition states of **Reaction 1-5** and normal-mode analysis reveals that they have only one imaginary frequency corresponding to the stretching modes of the coupling between breaking and forming bonds. The imaginary frequencies of the TS_{b-a}, TS_{b-c}, TS_{c-d}, TS_{b-e}, TS_{c-f} are $1853i$ cm^{-1}, $1599i$ cm^{-1}, $1856i$ cm^{-1}, $1670i$ cm^{-1} and $1796i$ cm^{-1}, respectively.

Since the structure of **a–f** belong to tautomers, they display similar IR spectra. The main absorption bands can be assigned as follows. The strong absorption bands between 3200~3700 cm^{-1} are the N-H stretching of amino group (or imino group). The values between 3150 and 3200 cm^{-1} are likely due to the N-H stretching of tetrazole

Table 4 The reaction energetic parameters (kcal·mol^{-1}) of each tautomerism of ATZ

Reactions	^rE	V_{MEP}	V_a^G
Reaction 1: b–a	10.94	63.19	59.39
Reaction 2: b–c	−2.67	49.52	45.66
Reaction 3: c–d	29.08	77.98	73.61
Reaction 4: b–e	33.42	58.12	54.90
Reaction 5: c–f	26.72	69.02	65.57

ring. The bands between 1650~1680 cm^{-1} and about 1590 cm^{-1} are assigned to the N-H bending and the endo-C-H bending, respectively. The N-N = N stretching bands are about 1300 cm^{-1}. The bands about 1260 cm^{-1} are likely due to the exo-C-N stretching. The values between 900~1200 cm^{-1} are likely due to the tetrazole ring stretching. The values below 780 cm^{-1} are assigned to the N-H rocking.

Energy barriers of tautomerism

The minimum-energy paths were obtained using the intrinsic reaction coordinate (IRC) theory at the MP2/6–311G** level of theory. The potential energy profiles were further refined using the CCSD (T)/6–311G**. We can see the transition states actually connect the relevant reactants and products. Table 4 presents the reaction energies (ΔE), the classical potential barriers (V_{MEP} = E_{ts} - $E_{reactants}$), ground-state vibrationally adiabatic energies (V_a^G), which

Table 3 Harmonic frequencies (cm^{-1}) and intensities (km/mol), for the reactants, products, and transition states at MP2/6–311G** method

| Species	Harmonic frequencies
a	154(19), 326(13), 430(19), 450(216), 654(53), 698(10), 708(14), 992(15), 1045(12), 1084(25), 1097(106), 1130(3), 1327(64), 1373 (42), 1415(2), 1793(500), 3578(10), 3717(96), 3718(128)
TS_{b-a}	$1853i$(734), 224(2), 486(184), 492(26), 549(81), 665(65), 689(6), 821(6), 977(84), 1017(5), 1037(16), 1073(22), 1161(85), 1218(13), 1258(37), 1383(3), 1462(30), 1699(409), 2092(82), 3622(26), 3709(125)
b	216(52), 301(2), 384(13), 565(60), 693(100), 718(5), 731(5), 820(190), 1075(20), 1114(12), 1131(8), 1167(16), 1211(11), 1383(1), 1516(27), 1621(58), 1672(179), 3581(28), 3683(35), 3689(101)
TS_{b-c}	$1599i$(184), 307(10), 332(30), 605(174), 670(82), 722(72), 739(56), 787(41), 966(17), 1051(3), 1066(6), 1120(5), 1138(10), 1231(18), 1456(5), 1566(123), 1663(201), 2424(121), 3613(52), 3728(47)
c	264(33), 320(16), 403(1), 554(53), 680(156), 724(68), 742(2), 791(128), 1044(7), 1054(7), 1117(4), 1125(26), 1226(26), 1335(9), 1410(11), 1520(2), 1576(98), 1662(193), 3606(32), 3674(123), 3718(35)
TS_{c-d}	$1856i$(335), 270(32), 483(184), 519(16), 628(185), 682(10), 716(2), 845(21), 950(80), 1019(53), 1064(2), 1082(34), 1194(41), 1229 (24), 1315(20), 1325(64), 1461(2), 1641(315), 2084(138), 3588(29), 3658(165)
d	208(1), 431(12), 512(81), 587(97), 666(466), 774(63), 822(78), 910(31), 993(9), 1092(29), 1095(17), 1157(65), 1321(33), 1353(17), 1397(29), 1488(14), 1748(201), 3553(24), 3568(70), 3610(64)
TS_{b-e}	$1670i$(1664), 193(7), 460(3), 484(15), 678(1), 702(1), 777(4), 1000(22), 1011(58), 1060(4), 1084(54), 1125(12), 1153(2), 1246(5), 1254(60), 1456(47), 1566(67), 1637(47), 2017(91), 3519(37), 3612(58)
e	232(16), 316(16), 681(24), 94(1), 1021(6), 1027(14), 1075(9), 1113(19), 1149(3), 1183(8), 1415(32), 1465(124), 1585(59), 1635(43), 1672(15), 3432(25), 3536(96), 3542(100)
TS_{c-f}	$1796i$(619), 215(9), 499(112), 550(60), 583(65), 674(26), 839(23), 974(129), 1008(39), 1031(8), 1142(29), 1171(50), 1230(45), 1362 (9), 1369(13), 1659(440), 2121(125), 3627(25), 3645(124)
f	201(6), 438(11), 454(61), 669(112), 709(38), 723(67), 750(3), 971(42), 974(82), 1060(7), 1140(77), 1266(14), 1307(41), 1382(25), 1434(28), 1555(6), 1764(482), 3580(16), 3652(127), 3701(112)

Reaction 1

Reaction 2

Reaction 3

Reaction 4
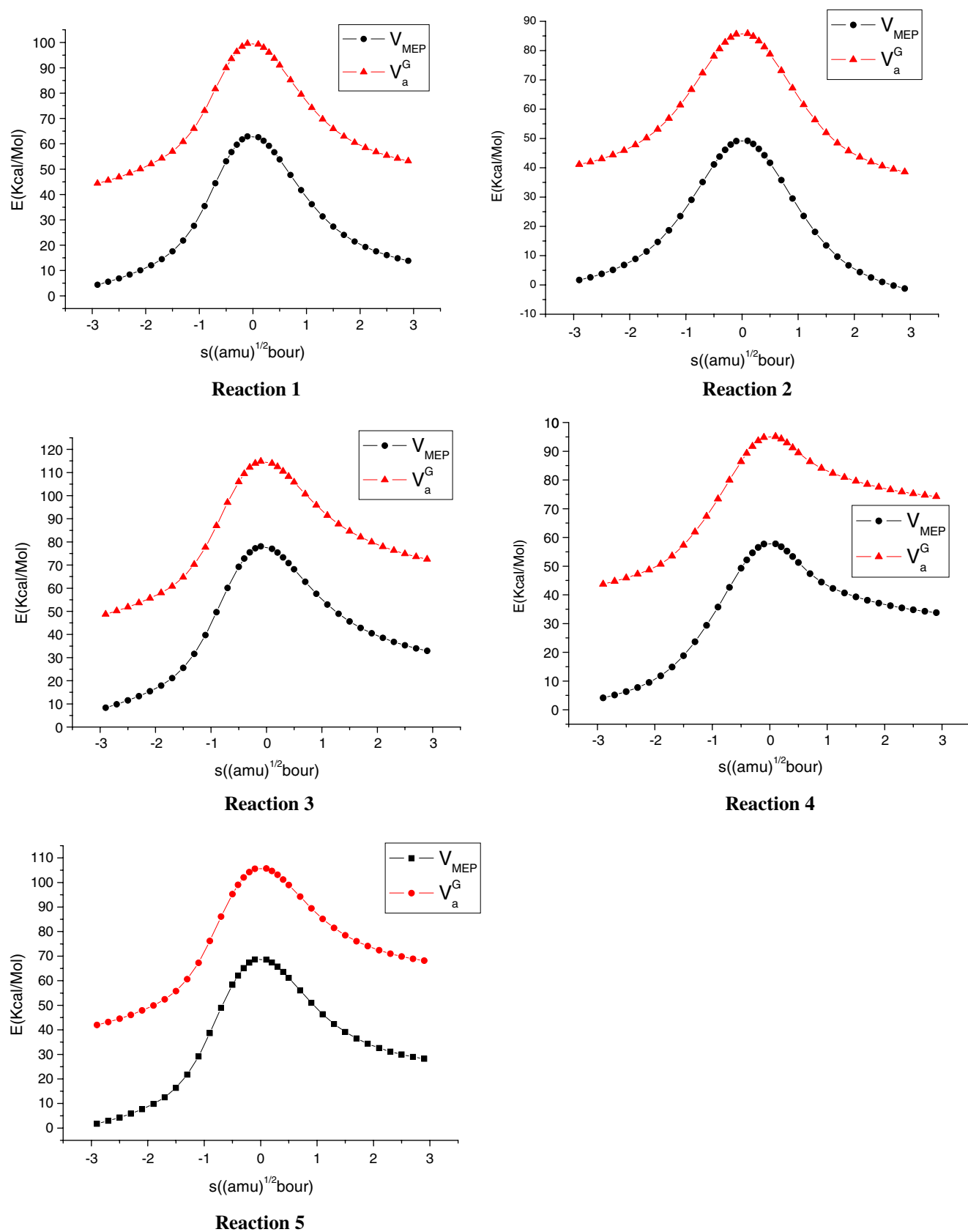
Reaction 5

Fig. 3 The vibrationally adiabatic ground-state potential energy curves (V_a^G) and the classical potential barriers (V_{MEP}) of the reactions as a function of s (amu)$^{1/2}$·bohr at the MP2/6–311G** level of theory
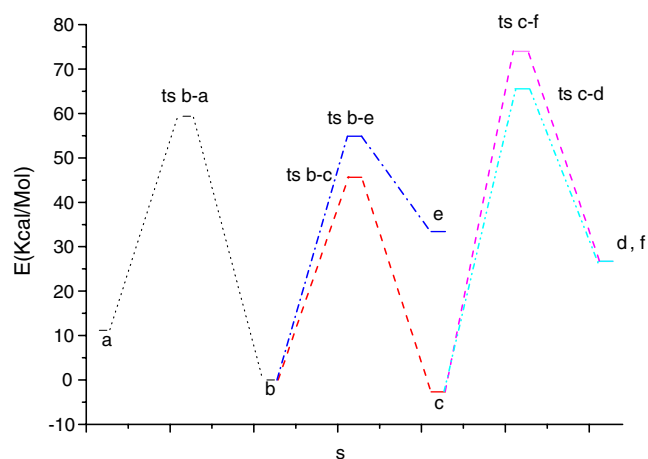
Fig. 4 The full potential energy surface representation of the tautomeric equilibrium and hydrogen shifts of ATZ at the CCSD(T)/ 6–311G**//MP2/6–311G** level of theory

were the corrected energies calculated using CCSD (T)/6–311G** with zero-point energies at MP2/6–311G** level (V_{MEP} + ZEP), and the reaction enthalpies (ΔH_{298K}^0). In the gas phase, the energy barrier (V_a^G) calculated for the rearrangement of **b** to **a** is 59.39 kcal/mol. The energy barrier for the **b** to **c** hydrogen shift is calculated to be 45.66 kcal/mol. It accords with the fact that **c** is more stable in the gas phase. The energy barrier for the rearrangements of **c** to **d** is 73.61 kcal/mol, larger than that for the hydrogen shift from **b** to **c**. The energy barrier of **c** to **f** is 65.57 kcal/ mol, smaller than **c** to **d**. The energy barrier of **b** to **e** is 54.90 kcal/mol that is smaller than the reaction from **b** to **a** and **c** to **d**. Although the compound of **a**, **d** and **f** are energetically less stable than the **b** and **c** species, they can be good candidates for experimental observation. In addition, **e** is a worthy topic for future research, too. We can also get a conclusion from Table 4 that **reaction 1**, **reaction 3**, **reaction 4**, and **reaction 5** are endothermic reactions while **reaction 2** is an exothermic reaction. These reactions may play an important role in both the atmosphere and in combustion systems of ATZ. Figure 3 gives the vibrationally adiabatic ground-state potential energy curves (V_a^G) and the classical potential barriers (V_{MEP}) of the reactions. In general, the smaller the imaginary frequencies are, the smoother the curves are. On the contrary, the curves are sharper. Figure 3 shows the curves are sharp that accords with the fact the imaginary frequencies of these reactions' transition states are big. As can be seen, all the $V_{MEP}(s)$ and V_a^G (s) curves are similar in shape, the positions of the maximum values of the two curves are located at the same position (s=0). This implies that the variational effect will be small for calculating the rate constants of the reactions. For all reactions, the effect of the ZEP correction is very obvious in the whole potential energy path. The full potential energy surface representation of the tautomeric

equilibrium and hydrogen shifts of ATZ at the CCSD(T) / 6–311G**//MP2/6–311G** level of theory are shown in Fig. 4, in which we can see the reactions more clearly.

Rate constants of tautomerism

The tautomerism reactions in this paper are typical hydrogen shift reactions. Therefore, it is necessary to quantify the competition, and it would be useful to have a more accurate estimate that includes the effect of tunneling. The expressions are derived by the TST, TST/Eckart, CVT, CVT/SCT, and CVT/ZCT methods using the optimized geometries obtained at the MP2/6–311G** and CCSD (T)/ 6–311G**. The rate constants at temperature range of 200~2500 K from different methods are shown in Fig. 5 and Table 5.

For **reaction 1,** the difference of the rate constants calculated by using the TST, TST/Eckart, CVT, CVT/SCT, and CVT/ZCT methods are significant only at lower temperatures and almost identical at high temperatures (T>500 K), so the tunneling effect has little effect at high temperatures. Through all the temperatures, the rate constants calculated by using TST and CVT are almost identical, but at low temperatures (200 K<T<500 K), the rate constants calculated by TST/Eckart, CVT/SCT and CVT/ZCT are quite different from the former. It is easily concluded that tunneling effect has a distinct effect on this reaction at low temperatures. The CVT rate constant and TST values are the same orders of magnitude smaller than other methods at lower temperatures, so the CVT and TST rate constants are lower than other methods in Fig. 5. Compare Arrhenius plots of all the rate constants under all kinds of methods, the bigger discrepancies should be due to the higher value of Ea and pre-exponential factor in the TST and CVT equations at lower temperatures. The smaller discrepancies should be due to the lack of a temperature in the pre-exponential factor at higher temperatures. In any case, our calculations indicate that the hydrogen shift of **reaction 1** plays a more important role in the tautomerism reactions of ATZ than that which was previously have believed. However, TST/Eckart rate constant is 3.67×10^{-26} confirms that the thermal reaction is far too slow to play a role in atmospheric chemistry at 300K. **Reaction 2** and **reaction 5** exhibit a similar trend with **reaction 1** during the whole temperature range.

For **reaction 3**, the rate constants calculated using the different methods are almost identical on the whole temperature range and there is only a little deviation at low temperatures (200 K<T<500 K) compared to the values calculated by TST method. A conclusion can be made that tunneling effect has smaller effect on this reaction at low temperatures than **reaction 1** and **reaction 2**. As we can see in Table 5, the rate constants increasing of
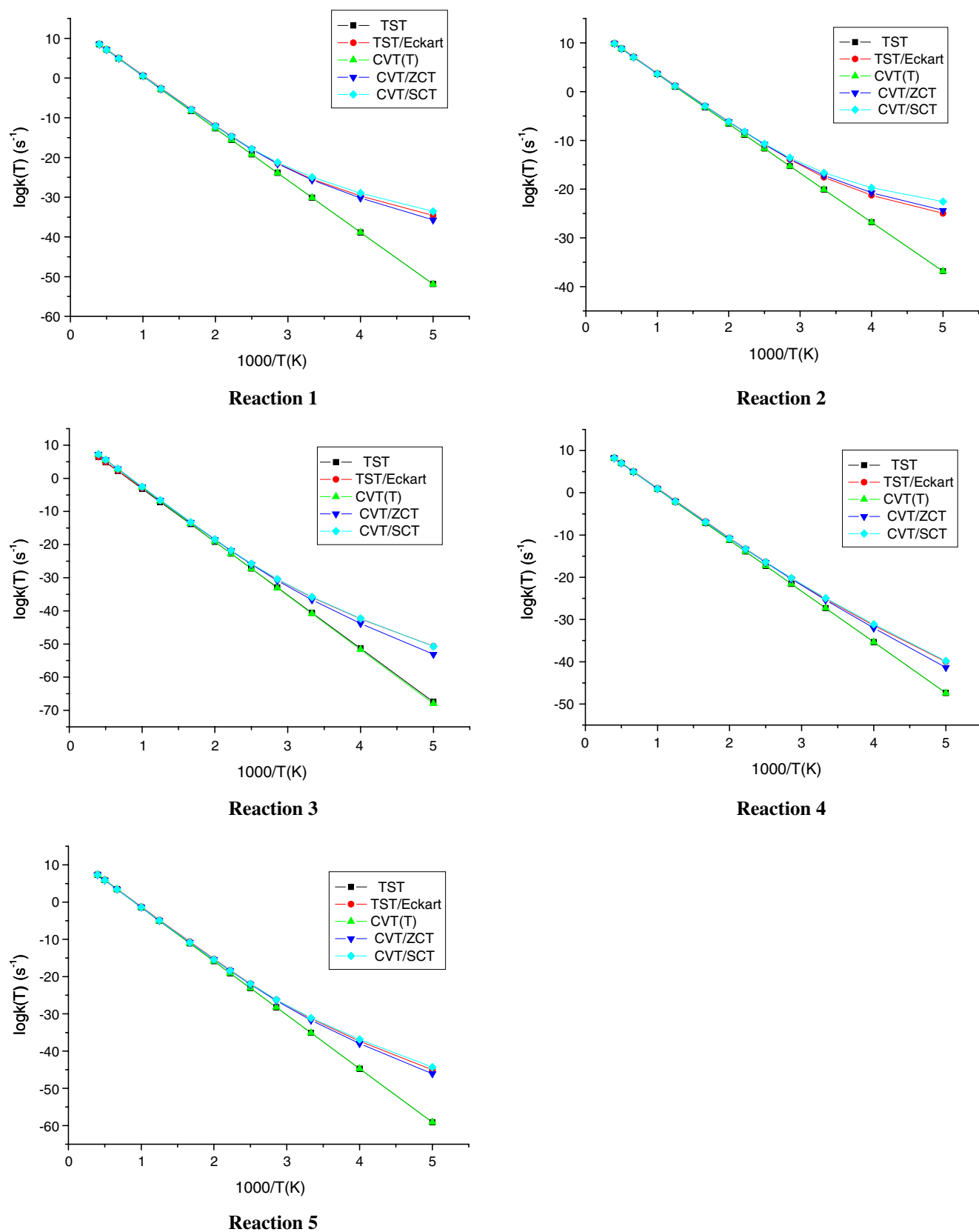
Fig. 5 Arrhenius plot of the rate constants calculated at the TST, TST/Eckart, CVT, CVT/SCT and CVT/ZCT, levels of theory. The rate constants are calculated based on the interpolated MEP at the MP2/6–311G** level of theory

Table 5 Rate constants (in s^{-1}) at temperature range of 200~2500 K from different methods

T(K)		TST	TST/Eckart	CVT	CVT/ZCT	CVT/SCT
Reaction 1	200	1.33E-52	2.45E-35	1.29E-52	1.81E-36	2.57E-34
	300	7.55E-31	3.67E-26	7.39E-31	2.29E-26	1.15E-25
	400	5.96E-20	1.51E-18	5.86E-20	1.12E-18	1.55E-18
	500	2.12E-13	1.08E-12	2.09E-13	7.73E-13	8.24E-13
	800	1.54E-03	2.91E-03	1.53E-03	2.11E-03	2.12E-03
	1000	3.12E+00	4.88E+00	3.09E+00	3.64E+00	3.65E+00
	1500	8.48E+04	1.10E+05	8.41E+04	8.70E+04	8.71E+04
	2000	1.45E+07	1.74E+07	1.44E+07	1.44E+07	1.44E+07
	2500	3.24E+08	3.72E+08	3.22E+08	3.18E+08	3.18E+08
Reaction 2	200	1.40E-37	1.09E-25	1.40E-37	4.36E-25	2.75E-23
	300	8.27E-21	2.85E-18	8.29E-21	6.48E-18	2.28E-17
	400	2.17E-12	1.61E-11	2.17E-12	1.61E-11	2.11E-11
	500	2.55E-07	8.13E-07	2.56E-07	6.68E-07	7.32E-07
	800	1.15E+01	1.90E+01	1.15E+01	1.46E+01	1.49E+01
	1000	4.27E+03	6.14E+03	4.28E+03	4.80E+03	4.85E+03
	1500	1.22E+07	1.51E+07	1.22E+07	1.24E+07	1.24E+07
	2000	6.73E+08	7.83E+08	6.73E+08	6.66E+08	6.68E+08
	2500	7.59E+09	8.54E+09	7.60E+09	7.46E+09	7.47E+09
Reaction 3	200	3.38E-68	2.01E-51	1.11E-68	7.65E-54	1.91E-51
	300	2.43E-41	1.17E-36	1.43E-41	2.07E-37	1.59E-36
	400	6.26E-28	1.63E-26	5.32E-28	1.09E-26	1.84E-26
	500	6.82E-20	3.50E-19	7.57E-20	3.52E-19	4.08E-19
	800	7.40E-08	1.40E-07	1.40E-07	2.48E-07	2.55E-07
	1000	7.44E-04	1.17E-03	1.79E-03	2.65E-03	2.69E-03
	1500	1.55E+02	2.01E+02	5.72E+02	7.10E+02	7.14E+02
	2000	6.78E+04	8.12E+04	3.38E+05	3.91E+05	3.92E+05
	2500	2.52E+06	2.90E+06	1.59E+07	1.77E+07	1.77E+07
Reaction 4	200	3.83E-48	1.02E-40	3.74E-48	4.47E-42	1.52E-40
	300	4.94E-28	7.35E-26	4.87E-28	4.00E-26	1.14E-25
	400	5.68E-18	4.51E-17	5.62E-18	3.41E-17	4.26E-17
	500	6.22E-12	2.12E-11	6.16E-12	1.59E-11	1.70E-11
	800	7.35E-03	1.25E-02	7.28E-03	9.50E-03	9.60E-03
	1000	7.96E+00	1.17E+01	7.89E+00	9.09E+00	9.13E+00
	1500	9.32E+04	1.17E+05	9.21E+04	9.54E+04	9.56E+04
	2000	1.04E+07	1.23E+07	1.03E+07	1.04E+07	1.04E+07
	2500	1.80E+08	2.04E+08	1.77E+08	1.76E+08	1.76E+08
Reaction 5	200	7.71E-60	8.68E-46	7.76E-60	8.33E-47	4.61E-45
	300	7.62E-36	5.03E-32	7.65E-36	2.03E-32	7.77E-32
	400	7.81E-24	1.32E-22	7.83E-24	8.11E-23	1.09E-22
	500	1.28E-16	5.72E-16	1.28E-16	3.76E-16	4.11E-16
	800	8.39E-12	2.29E-11	8.41E-12	1.55E-11	1.61E-11
	1000	3.87E-02	5.94E-02	3.87E-02	4.35E-02	4.39E-02
	1500	2.84E+03	3.64E+03	2.84E+03	2.87E+03	2.88E+03
	2000	7.99E+05	9.50E+05	7.98E+05	7.84E+05	7.86E+05
	2500	2.39E+07	2.73E+07	2.39E+07	2.33E+07	2.33E+07

reaction 3 is the fastest. All rate constants change fast as temperature increases, especially in the lower temperature range. Howerver, in the whole range analyzed, the TST and CVT figures are almost on the same orders at each temperature, being clearly smaller than the corresponding rate constants using other methods.

For **reaction 4**, the rate constants calculated by using the TST, TST/Eckart, CVT, CVT/SCT, and CVT/ZCT methods are almost identical at high temperatures (T>500 K) too, so tunneling effect has little effect at high temperatures. However, at low temperatures (200 K<T<500 K), the rate constants calculated by using TST/Eckart, CVT/SCT and CVT/ZCT methods are almost identical, and there is a little deviation compared to the values calculated by TST and CVT methods. A conclusion can be made that tunneling effect has some effects on this reaction at low temperatures

but not so distinct. The rate constants increase rapidly at lower temperature ranges, tunneling effect decelerates **reaction 4** by fewer orders of magnitude than other reactions, qualitatively, which is reasonable given the different curvatures of the minimum energy paths.

For all the reactions, the large curvatures in the TST/Eckart, CVT/ZCT, and CVT/SCT Arrhenius curves indicate that the tunneling effects are significant in the lower temperature range, respectively. The curves of the CVT are nearly superposition with the ones of the TST. The data calculated using these two methods have small difference. Therefore, for the reactions under consideration, the variational effects are small over the whole temperature range.

In Fig. 5, it can be seen that the reaction rate constants are underestimated by TST and CVT for all reactions. It is known that the Eckart method tends to overestimate the tunneling effects contribution especially at very low temperature. ZCT and SCT require geometry, energy, gradient, and Hessian information along the minimum energy path (MEP). The ZCT method restricts the tunneling effects path to be along the MEP, whereas the SCT method allows the tunneling path to cut corners due to the reaction path curvature. Among these methods, the SCT approach offers the most accurate treatment of tunneling effects [34, 35]. The calculations show if computational resources are limited, the present results support the use of the Eckart tunneling method and ZCT method. However, with the rapid progress in computer technology among direct dynamics methods such as used in this paper, SCT is the best method to calculate the kinetics of the reactions. Performing a standard three-parameter fit ($k = AT^n \exp(-E_a/RT)$, A: The preexponential factor, n: The fitting reaction grade, E_a: The fitting apparent activation energy) yields the CVT/SCT expressions calculated of the five reactions are:

Reaction 1: $k(T) = 2.296 \times 10^{-56} \times T^{19.921} \times e^{-(1.187 \times 10^4/T)} s^{-1}$.
Reaction 2: $k(T) = 3.238 \times 10^{-42} \times T^{15.942} \times e^{-(9.076 \times 10^4/T)} s^{-1}$.
Reaction 3: $k(T) = 8.021 \times 10^{-51} \times T^{18.329} \times e^{-(2.056 \times 10^4/T)} s^{-1}$.
Reaction 4: $k(T) = 2.164 \times 10^{-14} \times T^{7.654} \times e^{-(2.049 \times 10^4/T)} s^{-1}$.
Reaction 5: $k(T) = 1.786 \times 10^{-43} \times T^{16.051} \times e^{-(1.852 \times 10^4/T)} s^{-1}$.

Conclusions

The present study provides a detailed description of the tautomerism reactions with hydrogen shifts of ATZ, the geometry structures, the MEP were calculated at the MP2/6–311G** level of theory. The single-point energies were calculated at the CCSD (T)/6–311G**//MP2/6–311G** method of theory. The rate constants were evaluated using the TST, TST/Eckart, CVT, CVT/SCT, and CVT/ZCT methods. The performed calculation for ATZ tautomer in this study predicted the reasonable cyclic structure. In the gas phase, 2-H-5-amino-tetrazole (**c**) is predicted to be the dominant form. The stabilities of **b** and **c** can be ascribed to their aromatic characters with delocalization of the lone pair of the saturated nitrogen atom into the 5-membered ring to form 6π electron aromatic systems. Finally, our variational transition state theory calculations indicate that tunneling effects play a rather modest role in these hydrogen transfer reactions, such as **reaction 1**, **2, 3**, and **5**, while a smaller tunneling effect in **reaction 4**. It is expected that the present theoretical study may be useful for estimating the kinetics of the reactions over a wide temperature range where no experimental data are available.

References

1. Sivabalan R, Anniyappan M, Pawar SJ, Talawar MB, Gore GM, Venugopalan S et al (2006) J Hazard Mater A137:672–680 doi:10.1016/j.jhazmat.2006.03.038
2. Katritzky AR, Rogovoy BV, Kovalenko KV (2003) J Org Chem 68:4941–4943 doi:10.1021/jo0266543
3. Jime'nez V, Alderete JB (2006) J Mol Struct 775:1–7
4. Chen ZX, Xiao HM, Chin YN (1999) J Phys Chem A 103:8062–8066 doi:10.1021/jp9903209
5. Levchik SV, Ivashkevich OA, Balabanovich AI (1992) Thermochim Acta 207:115–130 doi:10.1016/0040-6031(92)80129-K
6. Jonassen HR, Pankert T, Henry RA (1967) Appl Spectrosc 21:89–91 doi:10.1366/000370267774385308
7. Nelson JH, Baglin FG (1972) Spectrosc Lett 5:101–105 doi:10.1080/00387017208064693
8. Murphy DB, Picard JP (1954) J Org Chem 19:1801–1817
9. Koz'min'ski W, Stefaniak L, Wiench JW (1995) Polish J Chem 69:74–79
10. Bocia W, Jaz'winsky J, Koz'minsky W, Stefaniak GA (1994) Webb J Chem Soc Perkin Trans 2:1327–1331 doi:10.1039/p29940001327
11. Barmin MI, Gromova SI, Kasatikova EL, Karaulova IB, V. MV (1992) Zhum Org Khim 28:1767–1771
12. Vander Putten N, Haeijdenrijk D, Schenk H (1974) Cryst Struct Commun :321–322
13. Palmer MH, Beveridge A (1987) J Chem Phys 111:249–255 doi:10.1016/0301-0104(87)80138-6
14. Ming WW, Regis LT, Curt W (1993) J Am Chem Soc 115:2465–2472 doi:10.1021/ja00059a048
15. Chen ZX, Xiao HM, Yang SL (1999) Chem Phys 250:243–248 doi:10.1016/S0301-0104(99)00336-5
16. Chen ZX, Xiao HM, Song WY (1999) J Mol Struct THEOCHEM 460:167–173 doi:10.1016/S0166-1280(98)00316-9
17. Chen ZX, Fan JF, Xiao HM (1999) J Mol Struct THEOCHEM 458:249–256 doi:10.1016/S0166-1280(98)00249-8
18. Chen ZX, Xiao HM (2000) Int J Quantum Chem 79:350–357 doi:10.1002/1097-461X(2000)79:6<350::AID-QUA3>3.0.CO;2-T
19. Frisch MJ, Trucks GW, Schlegel HB, Scuseria GE, Robb MA, Cheeseman JR (2003) GAUSSIAN 03, Revision A.1. Gaussian, Inc, Pittsburgh, PA

20. Frisch MJ, Head-Gordon M, Pople JA (1990) Chem Phys Lett 166:281–289 doi:10.1016/0009-2614(90)80030-H
21. Head-Gordon M, Pople JA, Frisch MJ (1988) Chem Phys Lett 153:503–509 doi:10.1016/0009-2614(88)85250-3
22. Petersson GA, Bennett A, Tensfeldt TG, Al-Laham MA, Shirley WA, Mantzaris J (1988) J Chem Phys 89:2193–2197 doi:10.1063/1.455064
23. Krishnan R, Binkley JS, Seeger R, Pople JA (1980) J Chem Phys 72:650–677 doi:10.1063/1.438955
24. Curtiss LA, Raghavachari K, Redfern PC, Rassolv V, Pople JA (1998) J Chem Phys 109:7764–7776 doi:10.1063/1.477422
25. Purvis GD, Bartlett RJ (1982) J Chem Phys 76:1910–1918 doi:10.1063/1.443164
26. Gonzalez C, Schlegel HB (1989) J Chem Phys 90:2154–2161 doi:10.1063/1.456010
27. Zhang SW, Truong TN (2001) VKLab version 1.0, University of Utah
28. Chuang YY, Corchado JC, Fast PL, Will J, Hu WP, Liu YP et al. (1999) P$_{OLYRATE}$, Program vision 8.2, Minneapolis
29. Truhlar DG, Isaacson AD, Garrett BC (1985) Theory of Chemical Reaction Dynamics, vol. 4. CRC Press, Boca Raton
30. Truong NT, Truhlar DG (1990) J Chem Phys 93:1761–1769 doi:10.1063/1.459103
31. Miller WH (1979) J Am Chem Soc 101:6810–6814 doi:10.1021/ja00517a004
32. Truhlar DG, Garrett BC (1984) Annu Rev Phys Chem 35:159–189 doi:10.1146/annurev.pc.35.100184.001111
33. Truong NT (1994) J Chem Phys 100:8014–8025 doi:10.1063/1.466795
34. Liu YP, Lynch GC, Troung TN, Lu DH, Truhlar DG, Garrett BC (1993) J Am Chem Soc 115:2408–2415 doi:10.1021/ja00059a041
35. Truhlar DG, Isaacson AD, Garrett BC (1982) J Phys Chem 86:2252–2263 doi:10.1021/j100209a021
36. Harmony MD, Laurie VW, Kuczkowski RL, Schwendeman RH, Ramsay UA, Lovas FL (1979) J. Phys. Chem. Ref. 8:679–721
37. Zhang LP, Tu YR Trans (1980) Foundation of Organ. Chem. (Theory and Application) Beijing: the Science Press
38. Palmer MH, Beveridge A (1987) J Chem Phys 111:249–261 doi:10.1016/0301-0104(87)80138-6